



3rd Workshop on Metallization for Crystalline Silicon Solar Cells,
25 – 26 October 2011, Charleroi, Belgium

Review on screen printed metallization on p-type silicon

S. Riegel*, F. Mutter, T. Lauermann, B. Terheiden, G. Hahn

University of Konstanz, Department of Physics, P.O. Box X916, 78457 Konstanz, Germany

Abstract

Advanced solar cell contacts feature local contacts to p- and p⁺-Si. In this review existing models for contact formation to p and p⁺-Si are presented.

The formation of the local Al BSF as applied in PERC like solar cell structures is inhibited by the formation of voids. It is shown that the formation of voids depends on process parameters and their influence on the contact formation is reviewed. Using an analytical model it is possible to predict the depth of the resulting Al BSF in dependence of the contact geometry and the peak firing temperature.

Contact formation to B doped Si with pure Ag paste results in high contact resistances whilst contact formation to Al doped Si with Ag paste is less difficult. The contact formation with Ag paste to B doped Si is enhanced by the addition of Al to the Ag paste.

© 2012 Published by Elsevier Ltd. Selection and/or peer review under responsibility of Guy Beaucarne

Open access under [CC BY-NC-ND license](https://creativecommons.org/licenses/by-nc-nd/4.0/).

Keywords: screen printing; p-type; crystalline silicon; solar cell; local contact, contact formation

*Corresponding author. Tel.: +49-7531-88-2074; fax: +49-7531-88-3895.

E-mail address: stefanie.riegel@uni-konstanz.de.

1. Introduction

One approach to reduce costs per wattpeak is increasing solar cell efficiency while keeping solar cell production costs moderate. Following this approach, advanced solar cell concepts like Passivated Emitter and Rear solar Cells (PERC, first published by [1]) [2-8], bifacial solar cells [9-14] and n-type solar cells [9, 14-19] gain more and more attention.

In the PERC concept the full area Al BSF (back surface field) is replaced by a dielectric passivation, which is locally opened for contact formation [1-8]. Contacts are formed by physical vapor deposition (CVD) of Al [1, 8] or screen printed Al [6-8, 20-30]. The dielectric passivation results in improved optical properties and less surface recombination [8]. But the local aluminum contact formation is challenging. The dielectric passivation layer must not be penetrated by Al [6]. Many authors report on the formation of voids underneath the Al contacts [7-8, 20-30] as well. If voids occur, only incomplete BSF formation takes place leading to enhanced surface recombination at the contacts and increased contact resistances.

Bifacial solar cells commonly use a diffused B BSF passivated by a dielectric layer instead of a full area Al BSF [9, 10, 12-14]. For rear side metallization a finger grid is applied similar to that used for front side metallization. Therefore, bifacial solar cells which collect light from the rear side as well feature improved optical properties and less surface recombination [10, 12, 13]. Like front side metallization finger grids applied on the rear side must provide low contact resistances and good line conductivity. But using the same metallization scheme as for highly P doped Si on the front side of Si solar cells for contact formation to highly B doped Si results in increased contact resistances [14, 19, 31-35].

Silicon solar cells produced from n-type Si substrates allow for higher efficiencies than those produced from p-type Si substrate as minority charge carrier lifetimes can be significantly larger [17, 36, 37]. Additionally, n-type Si is less sensitive to impurities [37]. Emitters for n-type solar cells may be fabricated by B diffusion or by screen print of Al paste [9, 14-16, 18, 19]. The latter is suitable for rear emitters only, if the Al paste is not removed. For contact formation to B diffused emitters the same difficulties as for B BSFs occur. An additional issue is the prevention of shunting of the emitter [14, 19, 31].

Besides their advantages, these novel solar cell concepts introduce new problems as described above. One problem crucial to all these concepts is the contact formation to p- and p⁺-Si [7-8, 14, 19-35]. Various authors have investigated different aspects of contact formation techniques to p- and p⁺-Si. This contribution gives an overview of recent models and the state of the art. In the first part of the contribution current models on local Al contact formation are summarized. Results from other authors concerning the influence of process parameters on the formation of local Al contacts are discussed. The second part deals with the impact of the doping element and the paste composition on the contact formation of screen printed Ag based metallization paste to highly p-doped Si.

2. Formation of a local Al BSF

In the PERC process rear contacts are formed locally after opening the dielectric layer. The opening of the dielectric may be done by laser, by using an etching paste or by masking of the dielectric and wet chemical etching. Afterwards the rear metallization – usually using Al - is carried out. The Al may be screen printed, evaporated or sputtered on the full area of the rear side or locally as lines or dots. Finally, the contacts are fired.

Detailed investigations on the contact formation between Al and Si, especially with focus on the diffusion of Si in Al, have already been carried out in semiconductor research [38-47]. Early work on the

Al-Si contact formation targeting the application in solar cells was done by Finetti et al. [48]. A model of the Al-Si alloying process with regard to screen printed Al is given by Huster [49] and Popovich et al. [50], based on the equilibrium phase-diagram of Al and Si of Murray and McAllister [51]. A detailed analysis of the formation of the Al-Si eutectic is published by Bock et al. [52], which gives an understanding of the high acceptor concentration normally found at the surface of aluminum-doped regions. Thickness homogeneity of full area Al BSFs is achieved by fast temperature ramp rates and a proper adjustment of the peak firing temperature and the amount of Al deposited [53-55].

The first solar cells to use a local Al BSF were published by von Finckenstein et al. [56] leading to efficiencies of up to 14.1% [57]. A first analysis of local Al contact formation is given by Agostinelli et al. [6] and Meemongkolkiat et al. [20]. To our knowledge the latter are the first to observe the formation of voids in local Al contacts and showed that they can be avoided by using a suitable Al paste. However, they do not comment on the proper paste composition. This is done by Rauer et al. [21] who proved that adding Si powder to the Al paste prevents the formation of voids and increases the BSF thickness. Further work targeting the influence of process steps and parameters on the contact formation is done by several authors. These investigations reveal that the method applied for opening the dielectric layer [22, 23], the contact geometry [7, 21, 23-29], the amount of Al [22, 24-29] and the firing profile [7, 23, 24, 27] influence the contact formation significantly. An extended analysis of local Al contact formation is done for example by Uruena et al. [8] with the result, that after opening of the dielectric barrier by laser, screen printing and firing of Al paste up to 60 μm deep Al-Si pyramids are seen. Uruena et al. [8] and Grasso et al. [30] propose simple models for the local Al alloying process which were extended by Lauer mann et al. [7] and Urrejola et al. [25-29]. An analytical model allowing to calculate the Al BSF thickness is introduced by Müller et al [58].

2.1. Model for local alloying

In a PERC like solar cell structure the rear side is locally contacted (first published by Blakers et al. [1]). The local contact formation is often realized by screen printing Al paste on a locally opened dielectric layer [6-8, 20-30]. The Al pastes used for this purpose do not fire through the dielectric [6-8, 20-30]. During the firing process the Al particles melt and start to alloy locally with the Si surface [49]. Due to the high solubility of Si in Al at temperatures above the eutectic point (e.g. [51]), Si from the Si substrate diffuses into the Al paste [7, 22, 26, 29] (see Fig. 1). For a full area contact the Si concentration in the liquid Al depends on the firing temperature and reaches its maximum at the peak firing temperature [49]. In case of a local Al-Si contact a concentration gradient between the high Si concentration above the contact openings and the Si-free Al between the openings. Hence, the Si diffuses laterally into the liquid Al. At peak temperature a lateral Gaussian distribution of the Si in the Al-Si alloy can be assumed [26].

The analytical model by Müller et al. [58] includes the influence of the peak firing temperature, the area over which the dielectric layer is opened and the shape of the openings (points or lines), but the shape of the firing profile is not taken into account. While the calculated depth of the Al BSF fits well with experimental data, the formation of voids cannot be explained within this model.

2.2. Influence of the contact size on ρ_C and R_C

Urrejola et al. [25] show that the specific contact resistivity ρ_C shows little variation with peak firing temperature. But the specific contact resistivity ρ_C increases with the dielectric barrier opening width d_1 while the total contact resistance R_C does not vary with the dielectric barrier opening width d_1 (see Figure 1). This may be explained by the fact, that for larger opening width d_1 the planar surface between

the Al-Si alloy half circles shows a relatively high contact resistance while the Al-Si alloy at the edges provides a low contact resistance [25].

2.3. Influence of the firing parameters

After firing the rear side of a solar cell with locally alloyed Al contacts shows dark-grey lines [6, 8, 26]. This is an Al-Si alloy indicating the approximate limit of the spread d_2 (see Figure 1) of Si in Al [6, 8, 26]. Urrejola et al. show that the line spreading depends linearly on the firing temperature [27].

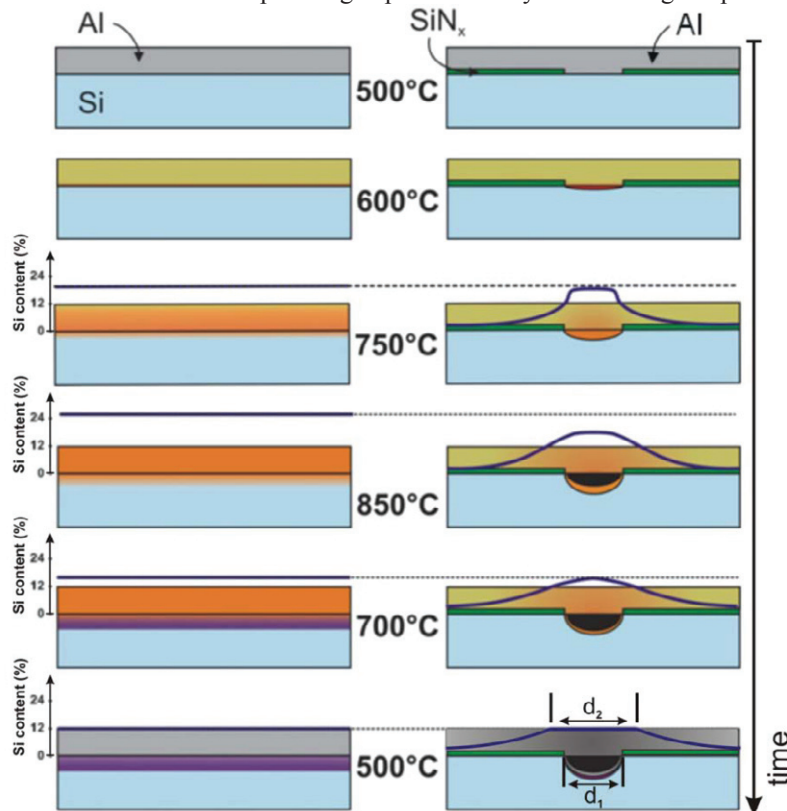


Fig. 1. : Model for the formation of a homogenous Al BSF (left) and local Al line contacts (right) as proposed by Lauermaann et al. [24]. Process time proceeds from top to bottom of the chart. The blue solid line represents the Si content as measured by [27]. The dashed line represents the Si solubility in Al at a given temperature. The dielectric barrier opening width is named d_1 . The spread of Si in the Al matrix is referred to as line spreading d_2 .

Besides the peak temperature the ramp-up and ramp-down rates, adjusted by the belt speed, influence the contact formation [22, 23]. The impact of the temperature ramp rates is investigated for constant peak temperature [23] as well as for constant thermal budget [22]. It depends on the shape of the dielectric barrier openings [23]. For line openings the resulting BSF becomes thinner when smaller ramp rates are applied and less voids are formed [22, 23]. In contrast, for point openings the BSF becomes thicker and more voids occur for smaller ramp rates [23].

2.4. Influence of the contact spacing and Al paste composition on the BSF thickness

If the contact spacing is too large, voids are formed [28]. Additionally, Rauer et al. show that the BSF thickness depends on the contact spacing [21]. For contact spacing below 500 μm , the BSF thickness increases significantly from zero up to 4 μm [21].

Meemongkolkiat et al. already showed in 2006, that a suitable additive can prevent the formation of voids and increase the thickness of the local BSF [20]. But it took until 2011 that Rauer et al. published that Si powder is a suitable additive for Al paste to increase the thickness of a local Al BSF and to reduce the depth of the local contacts [21]. Additionally they demonstrate a reduction in j_{0e} by increasing the Si content in the paste [21].

2.5. Influence of the method used for opening of the dielectric barrier

The formation of the BSF is influenced by the method used for opening of the dielectric barrier. Fang et al. [22] and Bähr et al. [23] observed thicker and more homogenous BSFs and less voids when an etching paste was applied to open the dielectric barrier instead of laser ablation using ns ($\lambda = 1064 \text{ nm}$ [23], 532 nm [22]) and fs ($\lambda = 1025 \text{ nm}$ [23]) lasers. The suboptimal BSF formation after laser ablation is traced back to an increased surface damage compared to dielectric barrier opening by an etching paste.

3. Contact formation to p^+ Si

Using n-type Si substrates the emitter formation may be done by B diffusion. In case of p-type Si substrate B diffusion is often applied for BSF formation in bifacial solar cell devices. As a finger grid provides little shading losses it is often applied as contact formation scheme to B doped p^+ -Si. Therefore, it is essential that the contact formation scheme allows for small contact and line resistances. Additionally, the diffusion profile must remain unchanged by contact formation.

Contacting p^+ -Si surfaces with Ag thick film paste results in a high ρ_C of $\sim 100 \text{ m}\Omega\text{cm}^2$ [14, 19, 31, 32]. The barrier height of the Ag - p-Si Schottky contact of 0.43 eV is near the critical value of 0.45 eV needed for a reasonable contact resistance [33, 59]. The barrier height can be reduced by increasing the acceptor impurity concentration under the contact [33, 59]. This can be achieved by adding Al to the Ag thick film paste and is first shown by Kopecek et al. [19].

Al contained in the metallization paste melts during the firing process. Where the liquid Al gets in contact with the Si wafer surface it forms Al doped regions on the Si wafer surface [32]. On Al doped Si surfaces the growth of Ag crystallites and therefore contact spots is enhanced [34]. The more Al is added to the Ag thick film paste, the more contact points are detected in the SEM surface analysis and smaller ρ_C are reached [14, 31, 35]. The contact points contain a relatively large concentration of Al [32, 34, 35]. An enhanced amount of Al is found at the wafer-contact point interface [32].

If the amount of Al added to the Ag thick film paste is too high, large Al spikes are identified in the SEM surface analysis [14, 31] leading to increased leakage currents or shunting of the solar cell [31]. This is due to the fact, that Al in the Ag/Al thick film paste is strongly attracted into the Si wafer and alloys deeply with the Si as observed for local Al contacts [7, 20-29]. The strong attraction of Al within the Ag/Al thick film paste by Si of the wafer can be lessened by adding some Si to the Ag/Al thick film paste as demonstrated by [14]. Thereby, the shunt conductance G_{SH} and the current density j_{01} are reduced [14], but the line resistance is increased.

3.1. Contact formation

3.1.1. Contact formation with Ag thick film paste to p⁺-Si (B, Al)

The specific contact resistance ρ_{C, Ag, p^+} of pure Ag thick film paste to highly boron doped Si ($N_{\text{surface}} = 9E18 \text{ cm}^{-3}$) is reported to be between 50 and 130 $\text{m}\Omega\text{cm}^2$ [14, 19, 31, 32]. After removing the Ag thick film paste in HF_{aq} (~5%) the Ag paste – Si interface contains very small Ag crystallites and inverted pyramids. With increasing firing temperature the number and size of the Ag crystals and inverted pyramids does not vary [32]. The pyramids are observed preferably at the $\langle 111 \rangle$ edges formed during sample processing by etching in hot NaOH_{aq} [34]. Enhanced growth of Ag crystallites along $\langle 111 \rangle$ oriented planes is observed for the Ag thick film firing process on n⁺Si as well [60, 61]. Butler et al. demonstrated by atomistic modeling that this enhanced Ag crystal growth can be explained by a reduction of the Schottky barrier of the Ag – Si contact down to 0.3 eV due to different charge densities at $\langle 111 \rangle$ and $\langle 110 \rangle$ interfaces [62].

For aluminum doped surfaces ($N_{\text{surface}} = 4E18 \text{ cm}^{-3}$) the Si wafer – Ag paste interface after removing the Ag thick film paste in HF_{aq} (~5%) looks different: The number and size of Ag crystallites is significantly increased and depends on the surface conditions of the wafers before metallization with Ag paste [32]. If the Ag paste is screen printed on the residuals of the Al-Si eutectic resulting from Al doping, more and larger Ag crystallites are detected. The Ag crystallites cluster along the lamellas of the Al-Si eutectic. Additionally, the Ag paste penetrates into the wafer at these structures. If the Al-doped surface is treated with NaOH_{aq} ($N_{\text{surface}} = 3E18 \text{ cm}^{-3}$), the Ag crystallites are smaller and cover the whole wafer surface regardless of the crystal orientation of the wafer surface [34].

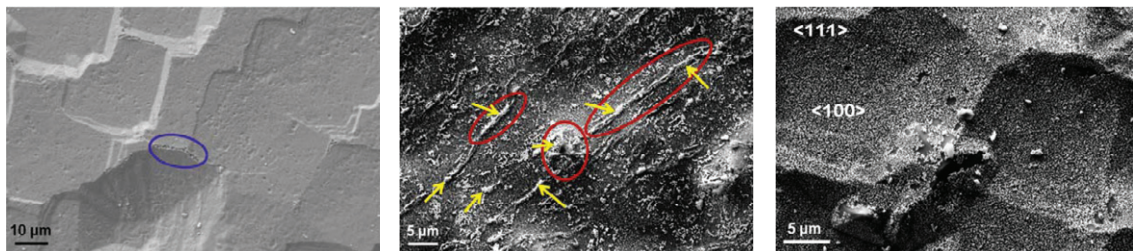


Fig. 2. : SEM micrographs of p⁺ Si layers metalized with Ag thick film paste. Ag thick film paste removed in HF_{aq} (5%). Left: highly B doped substrate: very few inverted pyramids are visible. The pyramids are mainly located at the edges between $\langle 100 \rangle$ and $\langle 111 \rangle$ surfaces formed during saw damage removal in NaOH_{aq} (e.g. blue oval). Middle: Al doped wafer surface, not wet chemically treated: Ag crystallites (e.g. yellow arrows) are preferably found along the lamellas (red ovals) of the Al-Si eutectic resulting from the Al alloying. Right: Al doped wafer surface etched in NaOH_{aq} before metallization. Very small Ag crystallites cover the whole wafer surface regardless of the crystal orientation of the surface [34].

3.1.2. Contact formation with Ag/Al thick film paste to p⁺-Si (B)

The addition of Al to Ag thick film paste results in a reduction of the specific contact resistance $\rho_{C, Ag/Al, p^+}$ down to 0.7 to 8 $\text{m}\Omega\text{cm}^2$ at optimum firing temperature [14, 19, 32, 35]. Additionally, the addition of Al to the Ag thick film paste leads to a more pronounced temperature dependency of the contact formation compared to pure Ag thick film paste. Already after drying the Ag/Al thick film paste at 290°C first contact spots are observed, even though the PbO is not molten yet [32]. After firing at 575°C most of the PbO is molten and contact spots containing Ag and Al are visible [32]. Furthermore, Al doped rectangles are found at the Si wafer surface [32]. For firing at 625°C all Al rectangles observed

include a contact spot [32]. Increasing the firing temperature further on does not change the contact structure, but leads to more and larger contact spots [32]. The contact spot size increases up to over 25 μm [40]. After firing at temperatures between 710 and 880°C Al precipitates at the Si wafer Ag/Al thick film paste interface [32].

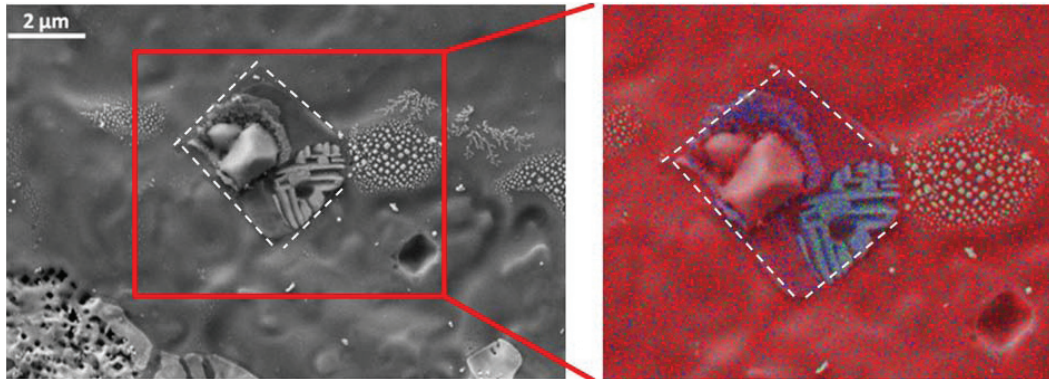


Fig. 3. : Ag/Al contact after etching in HF (5%), $T_{\text{peak}}=880^\circ\text{C}$. The area marked with the red box was measured with an EDX scan. Red: Si, green: Ag, blue: Al. One can see that the pellets in the right part of the contact consist of silver while the walls or lamellas in the middle of the red box consist of Al [32].

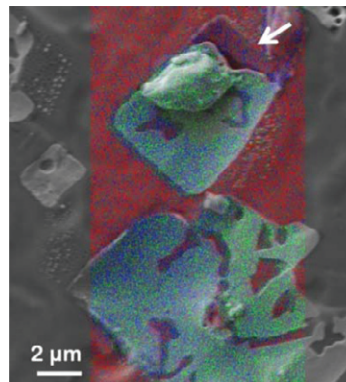


Fig. 4. : SEM micrograph and EDX scan of the contact area after etching in HF (5%), $T_{\text{peak}}=800^\circ\text{C}$. Red: Si, green: Ag, blue: Al. Most part of the contact area is filled with Ag and Al. In the lower right part of the scan area only Ag is detected. A part of the paste filling the upper contact is lifted. Therefore, the interface between Ag/Al thick film paste and the Si wafer is visible. At the Si-paste interface Al is detected (white arrow) [32].

3.2. Prevention of spiking

Contacting boron emitters with Ag/Al thick film pastes gives low R_S as mentioned above. But the inclusion of Al into the paste often leads to shunting of the cell or an increased j_{0e} as Al in the Ag/Al thick film paste is strongly attracted into the Si wafer. This problem can be overcome by adding of Si powder to the Ag/Al paste [14]. Lago et al. investigate a set of eight Ag based pastes for contacting boron

emitters containing different amounts of Al and Si. Large spikes (up to $5 \times 5 \mu\text{m}^2$ and $5 \mu\text{m}$ deep) are observed if the Al is not compensated by Si [14]. If Si is included in the paste no spikes are detected.

On cell level R_S is reduced from $\sim 2.5 \Omega\text{cm}^2$ down to $0.75 \Omega\text{cm}^2$ with increasing Al content [14]. Regarding the influence of Si, R_S is lowest for low Si content [14], but the higher the concentration of silicon in the metallization paste, the lower G_{SH} is observed [14]. The higher the Al content in the paste the more pronounced is the dependence of G_{SH} on the Si content in the paste [14]. The saturation current density j_{01} also shows a clear dependence on the Si content in the paste. Including more Si in the paste reduces the measured j_{01} [14].

4. Summary and conclusion

In this paper the existing phenomenological model for local Al contact formation and an analytical model to predict the BSF thickness depending on the peak firing temperature and the contact shape and size have been reviewed, and investigations concerning the influence of the process parameters on the contact formation have been summarized.

While ρ_C does not vary with peak firing temperature, the Al BSF thickness and the formation of voids change with increasing ramp rates. Whether the Al BSF formation and the formation of voids increase or decrease depends on the contact shape (lines or points). For a contact spacing smaller than $500 \mu\text{m}$ a significantly thicker BSF is observed, whereby the exact value may vary with firing parameters and Al metallization paste properties. Contact areas opened by etching with an etching paste reveal thinner and more homogenous BSFs and less voids than those opened by laser ablation.

Knowing the influence of process parameters in the contact formation allows for a phenomenological understanding of the contact formation and the definition of stable solar cell processes with homogenous BSF formation and the avoidance of voids. Though the influence of contact shape and peak firing temperature is understood in a more quantitative way, the quantitative understanding of the influence of the temperature ramp rates and the surface conditions is still lacking.

When contacting B doped Si with Ag metallization paste, the density of Ag crystallites or inverted pyramids does not increase with increasing peak firing temperature. Pyramids are preferably observed at the edges between $\langle 100 \rangle$ and $\langle 111 \rangle$ oriented surfaces. For Al doped Si significantly more Ag crystallites are observed than for B doped Si. The location of these crystallites does not depend on the Si crystal orientation. Adding Al to the Ag metallization paste reduces ρ_C by two orders of magnitude. Al in the metallization paste locally dopes the Si. Within these Al doped areas contact formation is enhanced and can lead to large (up to $5 \mu\text{m}$) inverted pyramids (“spikes”). Adding Si powder to the paste prevents the formation of spikes.

G_{sh} is increased and ρ_C and spiking are reduced by adding Al and Si powder to the Ag metallization paste. On cell level R_S is increased for increasing Si content in the Ag/Al metallization paste. To the knowledge of the authors studies regarding the line conductivity of Ag metallization pastes containing Al and Si powder have not been published yet. Additionally, further work regarding the influence of the doping element and the surface conditions on the contact formation to B doped Si is necessary.

Acknowledgements

The financial support from the BMU projects FKZ 0325168 and FKZ 0325079 is gratefully acknowledged in particular for the sample characterization. The content of this publication is the responsibility of the authors.

References

- [1] Blakers AW, Wang A, Mine AM, Zhao J, Green MA. 22.8% Efficient silicon solar cell. *Appl Phys Lett* 1989 ;**55**:1363-1365.
- [2] Dullweber T, Gatz S, Hannebauer H, Falcon T, Hesse R, Schmidt J et al. 19.4%-efficient large area rear-passivated screen-printed silicon solar cells. *Proc. 26th EU PVSEC Hamburg 2011*, 811-816.
- [3] Zielke D, Petermann JH, Werner F, Veith B, Brendel R, Schmidt J. 21.7% efficient PERC solar cells with AlO_x tunneling layer. *Proc. 26th EU PVSEC Hamburg 2011*, 1115-1119.
- [4] Urrejola E, Petres R, Glatz-Reichenbach J, Peter K, Wefringhaus E, Plagwitz H et al. High efficiency industrial PERC solar cells with all PECVD-based rear surface passivation. *Proc. 26th EU PVSEC Hamburg 2011*, 2233-2235.
- [5] Choulat P, Agostinelli G, Ma Y, Duerinckx F, Beaucarne G. Above 17% industrial type PERC solar cell on thin multi-crystalline silicon substrate. *Proc. 22nd EU PVSEC Milan 2007*, 1011-1014.
- [6] Agostinelli G, Szlufcick J, Choulat P, Beaucarne G. Local contact structures for industrial PERC-type solar cells. *Proc. 20th EU PVSEC Barcelona 2005*, 942-945.
- [7] Laueremann T, Lüder T, Scholz S, Raabe B, Hahn G, Terheiden B. Enabling dielectric rear side passivation for industrial mass production by developing lean printing-based solar cell processes. *Proc. 35th IEEE PVSC Honolulu 2010*, 28-33.
- [8] Uruena A, John J, Beaucarne G, Choulat P, Eyebeg P, Agostinelli G et al. Local Al-alloyed contacts for next generation Si solar cells. *Proc. 24th EU PVSEC Hamburg 2009*, 1483-1486.
- [9] Burgers AR, Geerlings LJ, Carr AJ, Gutjahr A, Saynova DS, Xiong X et al. 19.5% efficient n-type solar cells made in production. *Proc. 26th EU PVSEC Hamburg 2011*, 1144-1147.
- [10] Duran C, Buck T, Kopecek R, Libal J, Traverso F. Bifacial solar cells with boron back surface field. *Proc. 25th EU PVSEC Valencia 2010*, 2348-2352.
- [11] Cesar I, Romijn I, Borsa D, Galbiati G, Van Der Borg NJCM et al. Benchmark of open rear side solar cell with improved Al-BSF Process at ECN. *Proc. 23rd EU PVSEC Valencia 2008*, 1770-1775.
- [12] Riegel S, Gloger S, Raabe B, Hahn G. Comparison of the passivation quality of boron and Aluminum BSF for wafers of varying thickness. *Proc. 24th EU PVSEC Hamburg 2009*, 1596-1599.
- [13] Auriac N, Grange B, Cabal R, Maris-Froelicha A, Ribeyron PJ. High efficiency bifacial solar cell developed on monocrystalline Si and transferred to multicrystalline Si. *Energy Procedia* 2011;**8**:427-434.
- [14] Lago R, Pérez L, Kerp H, Freire I, Hoces I, Azkona N. Screen printing metallization of boron emitters. *Prog Photovolt Res Appl* 2010;**18**:20-7.
- [15] Richter A, Benick J, Kalio A, Seiffe J, Hörteis M, Hermle M et al. Towards industrial n-type PERT silicon solar cells: rear passivation and metallization scheme. *Energy Procedia* 2011;**8**:479-468.
- [16] Book F, Wiedenmann T, Schubert G, Plagwitz H, Hahn G. Influence of the front surface passivation quality on large area n-type solar cells with Alalloyed rear emitter. *Energy Procedia* 2011;**8**:487-492.
- [17] Glunz S, Benick J, Biro D, Bivour M, Hermle M, Pysch D et al. n-type silicon - enabling efficiencies > 20% in industrial production. *Proc. 35th IEEE PVSC Honolulu 2010*, 50-56.
- [18] Gong C, Van Kerschaver E, Robbelein J, Janssens T, Posthuma N, Poortmans J et al. Screen-printed aluminum-alloyed p⁺ emitter on high-efficiency n-type interdigitated back-contact silicon solar cells. *Electron Device Letters* 2010;**31**:576-578.
- [19] Kopecek R, Buck T, Libal J, Petres R, Röver I, Wambach K et al. Large area n-type multicrystalline silicon solar cells with B-emitter: efficiencies exceeding 14%. *Proc. 15th IPSEC, Shanghai 2005*.
- [20] Meemongkolkiat V, Nakayashiki K, Kim DS, Kim S, Shaik A, Kuebelbeck A. Investigation of modified screen-printing Al pastes for local back surface field formation. *Proc. 4th WCPEC Hawaii 2006*, 1338-1341.
- [21] Rauer M, Schmiga C, Woehl R, Rühle K, Hermle M, Hörteis M et al. Investigation of aluminum-alloyed local contacts for rear surface-passivated silicon solar cells. *IEEE J Photovolt* 2011;**1**:22-28.
- [22] Fang T, Lin C-M, Wang L-T, Tang W-C. Metallization of rear-side passivated solar cells: reducing cavities on local contacts. *Proc. 26th EU PVSEC Hamburg 2011*, 2220-2222.
- [23] Bähr M, Heinrich G, Doll O, Köhler I, Maier C, Lawerenz A. Differences of rear-contact formation between laser ablation and etching paste for PERC solar cells. *Proc. 26th EU PVSEC Hamburg 2011*, 1203-1209.
- [24] Laueremann T, Zuschlag A, Scholz S, Hahn G, Terheiden B. Influence of the contact geometry and sub-contact passivation on the performance of screen printed Al₂O₃ passivated solar cells. *Proc. 26th EU PVSEC Hamburg 2011*, 1137-1143.
- [25] Urrejola E, Peter K, Glatz-Reichenbach J, Wefringhaus E, Plagwitz H, Schubert G. Al-Si alloy formation in narrow p-Si contact areas. *Proc. 2nd Metallization Workshop Konstanz 2010*, 11-14.
- [26] Urrejola E, Peter K, Plagwitz H, Schubert G. Al-Si alloy formation in narrow p-type Si contact areas for rear passivated solar cells. *J Appl Phys* 2010;**107**:124519.
- [27] Urrejola E, Peter K, Plagwitz H, Schubert G. Silicon Diffusion in Aluminum for Rear Passivated Solar Cells. *Appl Phys Lett* 2011 ;**98** :153508.
- [28] Urrejola E, Peter K, Plagwitz H, Schubert G. Distribution of silicon in the aluminum matrix for rear passivated solar cells. *Energy Procedia* 2011;**8**:331-6.
- [29] Urrejola E, Peter K, Plagwitz H, Schubert G. Effect of gravity on the microstructure of Al-Si alloy for rear-passivated solar cells. *J Appl Phys* 2011;**110**:056104.

- [30] Grasso FS, Gautero L, Rentsch J, Preu R, Lanzafame R. Characterisation of local Al-BSF formation for PERC solar cell structures. *Proc 25th EU PVSEC Valencia 2010*, 371-374.
- [31] Kerp H, Kim S, Lago R, Recart F, Freire I, Pérez L et al. Development of screen printable contacts for p⁺ emitters in bifacial solar cells. *Proc. 21st EU PVSEC Dresden 2006*; 892-4.
- [32] Riegel S, Mutter F, Hahn G, Terheiden B. Contact formation in the silver/aluminum thick film firing process – a phenomenological approach. *Proc. 25th EU PVSEC Valencia 2010*, 2353-2356.
- [33] Mikhitarian V, Kravtchenko A, Garanzha S, Tchapygina O, Vityuk S, Schalko N et al. Lead free silver aluminum paste for crystalline silicon solar cells. *Proc. 21st EU PVSEC Dresden 2006*, 1129-1132.
- [34] Riegel S, Mutter F, Hahn G, Terheiden B. Influence of the dopant on the contact formation to p⁺-type silicon. *Energy Procedia* 2011;**8**:533-539.
- [35] Seyedmohammadi S, Graddy E, Shaik A. Screen printable Ag-Al metal pastes for p⁺ silicon application in solar cells. *Proc. 35th IEEE PVSC Honolulu 2010*, 003600-003603.
- [36] Glunz SW, Rein S, Lee JY, Warta W. Minority carrier lifetime degradation in boron-doped Czochralski silicon. *J. Appl. Phys.* 2001;**90**:2397-2404.
- [37] D. Macdonald, Geerlings JL. Recombination activity of interstitial iron and other transition metal point defects in p- and n-type crystalline silicon. *Appl. Phys. Lett.* 2004;**85**:4061-4063.
- [38] Bückle H. The Diffusion of Copper, Magnesium, Manganese and Silicone in Aluminium. *Zeitschrift für Elektrochem* 1943;**49**:238-42.
- [39] Yu AYC, Mead CA. Characteristics of Aluminum-Silicon Schottky Barrier Diode. *Solid State Electronics* 1970;**13**:97-104.
- [40] McCaldin JO, Sankur H. Diffusivity and Solubility of Si in the Al Metallization of Integrated Circuits. *Appl Phys Lett* 1971;**19**:524-7.
- [41] McCaldin JO, Sankur H. Precipitation of Si from the Al Metallization of Integrated Circuits. *Appl Phys Lett* 1972;**20**:171-2.
- [42] van Gorp GJ. Diffusion-limited Si precipitation in evaporated Al/Si films. *J Appl Phys* 1973;**44**:2040-50.
- [43] Chino K. Behavior of Al - Si Schottky barrier diodes under heat treatment. *Solid State Electronics* 1973;**16**:119-120.
- [44] Basterfield J, Shannon JM, Gill A. The nature of barrier height variations in alloyed Al-Si Schottky barrier diodes. *Solid State Electronics* 1975;**18**:290-1.
- [45] Mgbenu EN. Accelerated aging of Al/Ge and Al/Si thin film couples. *Thin Solid Films* 1980;**65**:267-74.
- [46] Garg N, Castleman LS, D'Antonio CD. Diffusion of silicon in aluminum-rich alloy thin films. *Thin Solid Films* 1984;**112**:317-28.
- [47] Paccagnella A, Ottaviani G, Fabbri P, Ferla G, Queirolo G. Silicon diffusion in aluminium. *Thin Solid Films* 1985 ;**128**:217-23.
- [48] Finetti M, Ostoja P, Solmi S, Soncini G. Aluminum-silicon ohmic contact on “shallow” n⁺p junctions. *Solid State Electronics* 1980;**23**:255-62.
- [49] Huster F. Investigation of the alloying process of screen printed aluminum pastes for the BSF formation on silicon solar cells. *Proc. 20th EU PVSEC Barcelona 2005*, 1466-9.
- [50] Popovich VA, Janssen M, Richardson IM, van Amstel T, Bennett IJ. Microstructure and Mechanical Properties of Aluminum Back Contact Layers. *Proc. 24th EU PVSEC Hamburg 2009*, 1453-8.
- [51] Murray JL and McAllister AJ. The Al-Si (aluminum-silicon) system. *Bulletin of Alloy Phase Diagrams* 1984;**5**:74-84.
- [52] Bock R, Schmidt J, Brendel R, Schuhmann H, Seibt M. Electron microscopy analysis of crystalline silicon islands formed on screen-printed aluminum-doped p-type silicon surfaces. *J Appl Phys* 2008;**104**:043701.
- [53] Narashima S, Rohatgi A, Weeber AW. An optimized rapid aluminum back surface field technique for silicon solar cells. *IEEE Transactions on Electron Devices* 1999;**46**:1363-1369.
- [54] Rohatgi A, Narashima S, Ebong AU, Doshi P. Understanding and implementation of rapid thermal technologies for high-efficiency silicon solar cells. *IEEE Transactions on Electron Devices* 1999;**46**:1970-1977.
- [55] Meemongkolkiat V, Nakayashiki K, Kim DS, Kopecek R, Rohatgi A. Factors limiting the formation of uniform and thick aluminum back surface field and its potential. *Journal of the Electrochemical Society* 2006;**153**:G53-G58.
- [56] von Finckenstein B, Spiegel M, Fath P, Bucher E. Local back surface field on thin low cost silicon solar cells. *Proc. 16th EU PVSEC Glasgow 2000*, 2100-2102.
- [57] von Finckenstein B, Horst H, Fath P, Bucher E. Thin mc low cost solar cells with 15% efficiency. *Proc. 28th IEEE PVSC Anchorage 2000*, 198-201.
- [58] Müller J, Bothe K, Gatz S, Brendel R. Modeling the formation of local highly aluminum-doped silicon regions by rapid thermal annealing of screen-printed aluminum. *Phys Status Solidi RRL* 2012; DOI 10.1002/pssr.201105611.
- [59] Fahrenbruch AL, Bube RH. Fundamentals of solar cells: Photovoltaic energy conversion. Academic Press, Orlando, Florida, USA, 1983.
- [60] Schubert G. Thick film metallisation of crystalline silicon solar cells : Mechanisms, models and applications. PhD thesis, Universität Konstanz, 2006.
- [61] Cabrera E, Olibet S, Glatz-Reichenbach J, Kopecek R, Reinke D, Schubert G. Current transport in thick film Ag metallization: Direct contacts at Silicon pyramid tips? *Energy Procedia* 2011;**8**:540-545.
- [62] Butler K, Vullum PE, Muggerrud AM, Cabrera E, Harding JH. Structural and electronic properties of silver/silicon interfaces and implications for solar cell performance. *Phys Rev B* 2011;**83**:235307.